Towards Large Eddy Simulation of Diesel Fuel Spray Using an Eulerian-Eulerian Approach

L. Martinez[1,*], A. Benkenida[1] and B. Cuenot[2]
1 : IFP, 1 & 4 avenue de Bois Préau
92852 Rueil-Malmaison Cedex, FRANCE
2 : CERFACS, 42 avenue G. Coriolis
31057 Toulouse Cedex, FRANCE

Abstract
The work described in this paper represents a validation step towards Large Eddy Simulation of Diesel fuel sprays using a two-fluid model based on the Mesoscopic Eulerian Formalism. This model has been extended to dense sprays by the addition of collision effects inspired from the kinetic theory. In order to avoid numerical and physical difficulties associated with simulating the flow at the nozzle exit, an alternate methodology is proposed which consists of starting the simulation at a given distance downstream from the nozzle exit. The dense spray model is then validated on the experience of a Diesel like spray injection into a dense air.

Introduction

Large Eddy Simulation (LES) appears to be a promising tool for the prediction of cycle to cycle variability in Internal Combustion (IC) Engines. Moreover, due to its potential to resolve large scale vortices and to predict the interaction between drops and the air (carrier phase), LES is of great interest for spray simulations [1].

This work is part of a program aimed at the application of LES to IC Engines. It is devoted to the development of a LES Eulerian-Eulerian approach for the simulation of Diesel like sprays. Eulerian methods are preferred to Lagrangian ones which are commonly used in CFD codes. The main drawback of Lagrangian methods is that, in order to achieve a satisfactory accuracy, a high particle number density is needed. This leads to a high computational cost which is unacceptable for industrial applications.
This paper is devoted to the presentation of a LES two-fluid model based on the mesoscopic eulerian formalism and its validation on a low pressure Diesel injection. For this purpose, the AVBP code [2], jointly developed by CERFACS and IFP, is used.

Specific Objectives

This work is a validation step towards Large Eddy Simulation of Diesel fuel sprays.

The first part of the paper presents the equations of conservation used in AVBP for both liquid and gas phase. The Mesoscopic Formalism as well as the developed collision model are presented.

A methodology based on an injector model to create boundary conditions shifted from the nozzle exit is described in the second part.

Finally, the new spray model (including collision effects) and boundary conditions are validated against the experiments [3]. For this purpose two computations have been performed and the results are compared to experimental measurements.

Furthermore, the contribution of the different physical mechanisms considered in this model is also analysed to determine which have the greatest influence on the spray dynamics.

Equations and models for the dispersed phase

A. *AVBP code and hypothesis for the simulations*

The AVBP code, used for the simulations, solves the compressible Navier Stokes equations for reactive two phase flows with low dissipation schemes adapted to LES on 3D unstructured hybrid grids. It allows the simulation of monodisperse or polydisperse evaporating two-phase flows. The simulations presented in this paper are performed in a monodisperse frame with neither evaporation nor gravity effect. The two phases are two-way coupled via drag force.

B. *Mesoscopic Eulerian Formalism*

Eulerian liquid conservation equations are based on the Mesoscopic Eulerian Formalism developed by Février et al.[4]. Unlike other Eulerian approaches, this method accounts for the Random Uncorrelated Motion (RUM) and was first developed for dilute two-phase flow.

In a cloud of particles, particles may have very different origins, therefore some particles may have very different velocities compared to the others even if they are close. The instantaneous velocity $\mathcal{V}_{p(t)}$ of a particle k positioned at X(t) can be decomposed into a mean component shared by all the particles (correlated velocity $u_{p(t)}$) and a component specific to the particle (uncorrelated velocity $\delta u_{p(t)}$):

$$\mathcal{V}_p^{(k)}(t) = u_p(\mathrm{X}^{(k)}(t),t) + \delta u_p^{(k)}(t) \qquad (1)$$

In order to obtain the information linked to the RUM, the probability density function (pdf) conditioned by a single realization of the carrier phase is introduced The principle for the establishment of the Eulerian liquid transport equation is the same as for the establishment of the Navier-Stokes equations by the kinetic theory [5].

* Corresponding author : lionel.martinez@ifp.fr

These equations are obtained by integration over the phase space of the Boltzmann-type equation of evolution of the pdf [4],[6],[7].

C. Filtering procedure

In a LES approach, only the large scale eddies are resolved whereas the small scale eddies are modeled. Differentiation between large and small scale terms is done by filtering. The filtering consists of applying a convolution product to the unfiltered variable f, with a spatial filter kernel $G_{\Delta f}$ of characteristic length Δ_f. The filtered quantity $\overline{f}$ is written as :

$$\overline{f}(x) = \int f(x) G_{\Delta_f}(x' - x) dx' \tag{2}$$

The Favre average is commonly used and allows to avoid density fluctuations. The Favre filtered quantity $\widehat{f}$ is written as :

$$\overline{\rho}\widehat{f}(x) = \int \rho f(x) G_{\Delta_f}(x' - x) dx' \tag{3}$$

For the dispersed phase equations, the density is replaced by the particle number density $\overline{n}_p$. Applying the Favre filter to the transport equation of droplet leads to the Eulerian filtered equations used in this work :

$$\frac{\partial}{\partial t}\alpha_p \rho_p + \frac{\partial}{\partial \mathrm{x}_j}\alpha_p \rho_p \hat{u}_{p,j} = 0 \tag{4}$$

where the liquid volumetric fraction α_p is defined as $\alpha_p = \overline{n}_p \pi d_p^{\,3}/6$, ρ_p is the mass density of the liquid which is considered constant, $\hat{u}_p$ is the filtered correlated velocity and d_p is the particle diameter. The filtered momentum equation is :

$$\begin{aligned}\frac{\partial}{\partial t}\alpha_p \rho_p \hat{u}_{p,i} + \frac{\partial}{\partial \mathrm{x}_j}\alpha_p \rho_p \hat{u}_{p,j}\hat{u}_{p,i} = -\frac{\alpha_p \rho_p}{\tau_p}\left(\hat{u}_{p,i} - \hat{u}_{f,i}\right) \\ -\frac{\partial}{\partial \mathrm{x}_j}\mathcal{T}_{p,j} + \frac{\partial}{\partial \mathrm{x}_j}\widehat{\delta\Sigma}_{p,ij}\end{aligned} \tag{5}$$

The first term on the right hand side (rhs) is the drag force, τ_p is the particle relaxation time defined as $\tau_p = \frac{\rho_p d_p^2}{18\mu_f}$ where μ_f is the fluid viscosity, and $\mathcal{T}_{p,ij}$ is the particle subgrid stress. The last term is the flux of the stress tensor $\widehat{\delta\Sigma}_{p,ij}$ defined from the filtered Random Uncorrelated Velocity (RUV) tensor $\widehat{\delta\mathcal{R}}_{p,ij}$ where $\widehat{\delta\mathcal{R}}^*_{p,ij}$ is its deviatoric part. The stress tensor reads $\widehat{\delta\Sigma}_{p,ij} = -2/3\alpha_p\rho_p\widehat{\delta\theta}_p\delta_{ij} - \alpha_p\rho_p\widehat{\delta\mathcal{R}}^*_{p,ij}$. The filtered Random Uncorrelated Energy (RUE) $\widehat{\delta\theta}_p$ is defined as the half of the RUV tensor trace [8],[9]. The term $2/3\widehat{\delta\theta}_p\alpha_p\rho_p$ is a dilatation term similar to a pressure written as $\mathcal{P}_{\mathrm{RUV}}$. The transport equation of RUE is :

$$\begin{aligned}\frac{\partial}{\partial t}\alpha_p\rho_p\widehat{\delta\theta}_p + \frac{\partial}{\partial \mathrm{x}_j}\alpha_p\rho_p\hat{u}_{p,j}\widehat{\delta\theta}_p = -2\frac{\alpha_p\rho_p}{\tau_p}\widehat{\delta\theta}_p - \frac{\partial}{\partial \mathrm{x}_j}\alpha_p\rho_p\widehat{\delta\mathcal{K}}_{p,iij} \\ -\widehat{\delta\Sigma}_{p,ij}\frac{\partial}{\partial \mathrm{x}_j}\hat{u}_{p,j} + \Pi_{\delta\theta_p} - \frac{\partial}{\partial \mathrm{x}_j}Q_{p,j}\end{aligned} \tag{6}$$

The first term of the rhs is the RUE loss by drag force. It means that particles which are submitted to the carrier phase influence tend to have the same velocity. The second term is a diffusion term while the third term is a production term. The fourth and fifth terms are respectively production and diffusion terms by subgrid scales.

D. Closure models for RUV terms

The terms $\widehat{\delta\mathcal{R}}^*_{p,ij}$ and $\widehat{\delta\mathcal{K}}_{p,ij}$ are modeled, respectively, by a viscous assumption and a diffusion term similar to Ficks' law [9] :

$$\widehat{\delta\mathcal{R}}^*_{p,ij} = -2\hat{\nu}_{\mathrm{RUV}}\left(S_{p,ij} - S_{p,mm}\delta_{ij}/3\right) = -2\hat{\nu}_{\mathrm{RUV}}S^*_{p,ij} \tag{7}$$

$$\widehat{\delta\mathcal{K}}_{p,iij} = -\hat{\kappa}_{\mathrm{RUV}}\left(\frac{\partial\hat{\theta}_p}{\partial \mathrm{x}_j}\right) \tag{8}$$

where $S_{p,ij} = \frac{1}{2}\left(\frac{\partial\hat{u}_{p,i}}{\partial \mathrm{x}_j} + \frac{\partial\hat{u}_{p,j}}{\partial \mathrm{x}_i}\right)$ is the rate strain tensor, $\hat{\nu}_{\mathrm{RUV}}$ is the RUV viscosity and $\hat{\kappa}_{\mathrm{RUV}}$ is a diffusion coefficient :

$$\hat{\nu}_{\mathrm{RUV}} = \frac{\tau_p}{3}\widehat{\delta\theta}_p \tag{9}$$

$$\hat{\kappa}_{\mathrm{RUV}} = \frac{10}{27}\tau_p\widehat{\delta\theta}_p \tag{10}$$

These models have been validated, a priori, in gas particle homogeneous isotropic turbulence [7].

E. Closure models for subgrid terms

Subgrid terms models from Riber et al. [6] are used for the computations. The SGS tensor $\mathcal{T}_{p,ij}$ is decomposed into two parts, the diagonal part equivalent to a subgrid pressure $\mathcal{P}_{\mathrm{SGS}}$ and the non-diagonal part equivalent to a subgrid viscous tensor $\mathcal{T}^*_{p,ij}$:

$$\mathcal{T}_{p,ij} = P_{SGS}\delta_{ij} + \mathcal{T}^*_{p,ij} \tag{11}$$

The closures used in this work for the subgrid production and diffusion terms can be found in [6].

F. Collision model

Closures for RUV terms are linked to the drag force and so to the correlation with the carrier phase. Thus the drag force is the predominant effect which is taken into account for the evolution of the RUM. This hypothesis is only valid when the relaxation time is the minimum relevant time scale. In the dense zone of the spray, the collision time can be smaller than the relaxation time. It means that the droplets do not have the time to be influenced by the carrier phase. Therefore one has to adapt the equation and hypothesis for the closure of the RUV terms. For this purpose an analogy is proposed between the RUE and the granular temperature often used for circulating fluidized beds simulation [10],[11]. The principles and developments of the models are reviewed in [11]. The collision time [5] reads $\tau_c = \frac{d}{24 g_0 \alpha_p}\sqrt{\frac{3\pi}{\widehat{\delta\theta}}}$ where $g_0 = \left(1 - \frac{\alpha_p}{\alpha_m}\right)^{-2.5\alpha_m}$ is the radial distribution function [12] with $\alpha_m = 0.7$.

The collision effects change the modelling of the RUV viscosity and diffusion defined in Eq. (9) and (10) to introduce the collisional time. The subscript *c* is used for the corrected terms $\hat{\nu}_{\mathrm{RUV}c}$ and $\hat{\kappa}_{\mathrm{RUV}c}$:

$$\hat{\nu}_{\mathrm{RUV_c}} = \frac{1}{3}\widehat{\delta\theta}_p\left(1+\alpha_p g_0 A\right)\Big/\left(\frac{1}{\tau_p}+\frac{B}{2\tau_c}\right) \quad (12)$$

$$\hat{\kappa}_{\mathrm{RUV}c} = \frac{2}{3}\widehat{\delta\theta}_p\left(1+\alpha_p g_0 C\right)\Big/\left(\frac{9}{5\tau_p}+\frac{D}{\tau_c}\right) \quad (13)$$

where A, B, C and D are numerical functions depending on the restitution coefficient e [11]. Additional terms, linked to collision effects, also appear in the stress and diffusive tensors :

Collisional diffusivity :

$$\hat{\kappa}_{coll} = \alpha_p g_0(1+e)\left(\frac{6}{5}\hat{\kappa}_{\mathrm{RUV}c} + \frac{4}{3}d_p\sqrt{\frac{2\widehat{\delta\theta}_p}{3\pi}}\right) \quad (14)$$

Collisional viscosity :

$$\hat{\nu}_{coll} = \frac{4}{5}\alpha_p g_0(1+e)\left(\hat{\nu}_{\mathrm{RUV}c} + d_p\sqrt{\frac{2\widehat{\delta\theta}_p}{3\pi}}\right) \quad (15)$$

Collisional pressure :

$$P_{coll} = \frac{4}{3}{\alpha_p}^2\rho_p g_0(1+e)\widehat{\delta\theta_p} \quad (16)$$

Bulk viscosity :

$$\xi_{coll} = \frac{4}{3}{\alpha_p}^2\rho_p g_0(1+e)d_p\sqrt{\frac{2\widehat{\delta\theta_p}}{3\pi}} \quad (17)$$

The new effective stress and diffusive tensors, taking into account collision effects, are then :

$$\widehat{\delta\Sigma}^{tot}_{p,ij} = -\left(\mathcal{P}_{\mathrm{RUV}} + \mathcal{P}_{\mathrm{coll}} - \xi_{\mathrm{coll}}\mathcal{S}_{p,mm}\right)\delta_{ij} + 2\alpha_p\rho_p\left(\hat{\nu}_{\mathrm{RUV_c}} + \hat{\nu}_{\mathrm{coll}}\right)\mathcal{S}^*_{p,ij} \quad (18)$$

$$\widehat{\delta\mathcal{K}}^{tot}_{p,iij} = -\left(\hat{\kappa}_{\mathrm{RUV_c}} + \hat{\kappa}_{\mathrm{coll}}\right)\left(\frac{\partial\hat{\theta}_p}{\partial \mathrm{x}_j}\right) \quad (19)$$

Thus Eq. (5) and (6) become respectively Eq. (20) and (21) :

$$\frac{\partial}{\partial t}\alpha_p\rho_p\hat{u}_{p,i} + \frac{\partial}{\partial \mathrm{x}_j}\alpha_p\rho_p\hat{u}_{p,j}\hat{u}_{p,i} = -\frac{\alpha_p\rho_p}{\tau_p}\left(\hat{u}_{p,i}-\hat{u}_{f,i}\right) + \underbrace{\frac{\partial}{\partial \mathrm{x}_j}2\alpha_p\rho_p\left(\hat{\nu}_{\mathrm{RUV_c}}+\hat{\nu}_{\mathrm{coll}}\right)\mathcal{S}^*_{p,ij}}_{1} \underbrace{-\frac{\partial}{\partial \mathrm{x}_i}\mathcal{P}_{\mathrm{RUV}}}_{2} \underbrace{-\frac{\partial}{\partial \mathrm{x}_i}\mathcal{P}_{\mathrm{coll}}}_{3} \underbrace{-\frac{\partial}{\partial \mathrm{x}_i}\mathcal{P}_{p,\mathrm{SGS}}}_{4} \underbrace{-\frac{\partial}{\partial \mathrm{x}_j}\mathcal{T}^*_{p,ij}}_{5} + \frac{\partial}{\partial \mathrm{x}_i}\left(\xi_{\mathrm{coll}}\mathcal{S}_{p,mm}\right) \quad (20)$$

$$\frac{\partial}{\partial t}\alpha_p\rho_p\widehat{\delta\theta_p} + \frac{\partial}{\partial \mathrm{x}_j}\alpha_p\rho_p\hat{u}_{p,j}\widehat{\delta\theta_p} = \Pi_{\delta\theta_p} - \frac{\partial}{\partial \mathrm{x}_j}\mathrm{Q}_{p,j} - 2\frac{\alpha_p\rho_p}{\tau_p}\widehat{\delta\theta_p} + \alpha_p\rho_p\frac{\left(e^2-1\right)}{3\tau_c}\widehat{\delta\theta_p} - \frac{\partial}{\partial \mathrm{x}_j}\alpha_p\rho_p\widehat{\delta\mathcal{K}}^{tot}_{p,iij} - \widehat{\delta\Sigma}^{tot}_{p,ij}\frac{\partial}{\partial \mathrm{x}_j}\hat{u}_{p,j} \quad (21)$$

This model can be seen as an extension of the dilute model. When the liquid void fraction tends to zero, the closures of the dilute model are recovered.

G. Gas phase equations

With the same filtering procedure we obtain the filtered equations for the gas phase from the classical volume averaged Eulerian equations [13] :

$$\frac{\partial}{\partial t}\alpha_f\overline{\rho_f} + \frac{\partial}{\partial \mathrm{x}_j}\alpha_f\overline{\rho_f}\hat{u}_{f,j} = 0 \quad (22)$$

$$\frac{\partial}{\partial t}\alpha_f\overline{\rho_f}\hat{u}_{f,i} + \frac{\partial}{\partial \mathrm{x}_j}\alpha_f\overline{\rho_f}\hat{u}_{f,j}\hat{u}_{f,i} = -\alpha_f\frac{\partial}{\partial \mathrm{x}_i}\overline{\mathcal{P}} + \frac{\partial}{\partial \mathrm{x}_j}\alpha_f\overline{\tau}_{ij} - \frac{\partial}{\partial \mathrm{x}_j}\mathcal{T}_{f,ij} + \frac{\alpha_p\rho_p}{\tau_p}\left(\hat{u}_{p,j}-\hat{u}_{f,j}\right) \quad (23)$$

$$\frac{\partial}{\partial t}\alpha_f\overline{\rho_f}\hat{\mathcal{E}}_f + \frac{\partial}{\partial \mathrm{x}_j}\alpha_f\overline{\rho_f}\hat{u}_{f,j}\hat{\mathcal{E}}_f = \frac{\partial}{\partial \mathrm{x}_j}\overline{\left(-\alpha_f\mathcal{P}+\alpha_f\tau_{ij}\right)u_{f,j}} + \frac{\partial}{\partial \mathrm{x}_j}\mathrm{Q}_{f,j} + \frac{\alpha_p\rho_p}{\tau_p}\left(\hat{u}_{p,j}-\hat{u}_{f,j}\right)\hat{u}_{p,j} \quad (24)$$

where the subscript f indicates the fluid phase, $\hat{\mathcal{E}}_f$ stands for the gas phase total filtered non chemical energy, $\mathcal{P}$ is the pressure and τ the viscous tensor. The SGS tensor $\mathcal{T}_{f,ij}$ is modeled via the classical Smagorinsky model. The term $\mathrm{Q}_{f,ij}$ is the subgrid scale heat flux vector.

Injector model for shifted boundary conditions

A. Principle of the shifted boundary condition

Numerical and physical constraints lead to high difficulties in simulating the liquid behavior at the nozzle exit.

Firstly, the main difficulty is related to the large range of physical scales that has to be solved when a complete simulation starting from the injection nozzle is performed. As a result of the small diameters of injectors, starting the simulation from the nozzle exit involve a very high computational cost.

Secondly, starting from the nozzle exit implies the addition of primary break up effects in the equations. Such effects are not easy to model nor to validate.

Consequently, we choose to use an inlet boundary condition at 10D from the nozzle exit. It means that the flow at the nozzle exit and primary break-up are not considered, which leads to reasonable computational costs. This distance is chosen so that primary break-up is completed. Smallwood et al. [13] have observed from experimental measurements that Diesel sprays are totally atomised at 10D from the nozzle exit. This is confirmed by the analysis of Ueki et al. [15] who concluded that primary break-up occurred between 2.5D and 7.5D.

B. Hypothesis for creating the shifted boundary conditions

Gaussian profiles of axial droplet velocity and volumetric liquid fraction are assumed and used as boundary conditions at 10D. These profiles are parameterized via an injector model which is able to calculate the spray angle, velocity and liquid volumetric fraction at the required distance.

The exit velocity is calculated via the model of Sarre et al. [15] which considers whether the flow is cavitating or not. The spray angle, at the nozzle exit, is assumed to be due to the primary atomization whose energy comes from the cavitation [17] and the turbulence generated into the nozzle [18]. The spray angle at 10D is modified by accounting for the aerodynamic effects that could increase the angle. Volumetric liquid fraction is deduced by conservation of the mass flow rate between the nozzle exit and 10D.

This injector model has been validated on different types of injectors and can produce accurate boundary conditions in order to initiate the two-phase flow.

Results and discussions

A. Experiment of Diesel like injection into dense air

To validate the dense spray model, the experiment of Chaves [3] is investigated as a first step. It corresponds to a Diesel like liquid injection without cavitation at a moderate pressure (ΔP = 10MPa) into a quiescent dense air (3MPa). The injector diameter is D=200µm. The measurements are performed when the injection reaches a quasi-steady state. Bernoulli velocity is 154.7m/s for this case. Radial profiles of axial velocity are provided at 10D and 100D from the nozzle exit. Profiles at 10D allow the validation of the injector model while the profiles at 100D allow the validation of the 3D LES simulation. The picture of the spray (Figure 1) gives an indication on the angle of the spray and its structures.

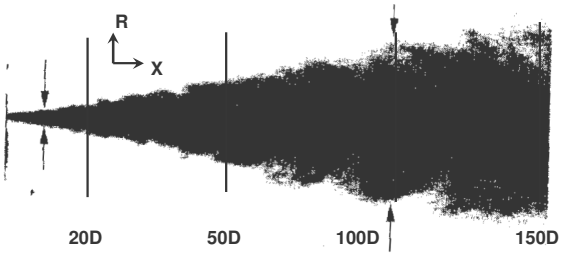

Figure 1 : Picture of the spray from Chaves [3] and position of the different cut lines.

B. Mesh and boundary conditions

A tetrahedral 3D mesh (Figure 2) is used for the calculations. It is composed of 518000 nodes, with a minimum edge length of 100µm. The shifted boundary condition is made possible by the addition of a cone, in the mesh, which can be seen in Figure 2.

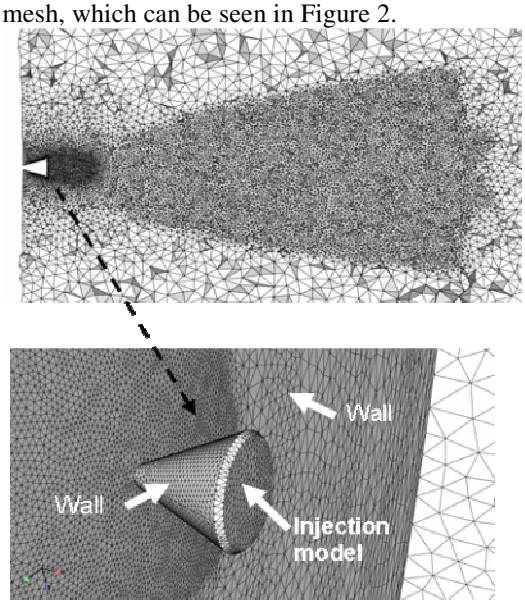

Figure 2 : Cross section of the mesh and view of the cone dedicated to the shifted boundary conditions.

The injector model presented previously is used for the generation of the boundary conditions. Figure 3 shows the axial velocity profile obtained by the model. This profile is compared to experimental measurement at 10D. We can see that except for the point at the radial distance of 1.5D, the profile obtained by the model is very close to the experiment. The mean velocity profile obtained by Chaves overestimates the width of the spray at 10D compared to the one measured on the spray picture. With the injection model, the width of the spray is respected.

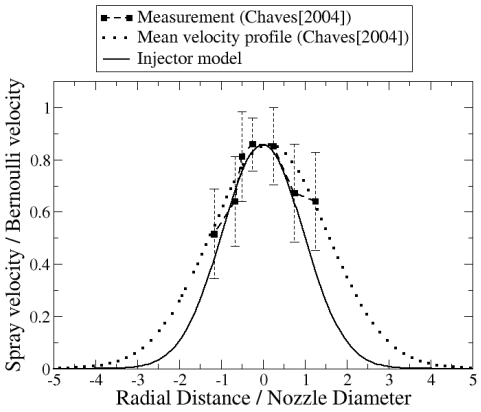

Figure 3 : Radial distribution of normalised axial droplet velocity at 10D from the injector nozzle.

Two computations have been performed : the first one uses a constant droplet diameter (20µm) , and the second is based on a Gaussian radial distribution of this diameter at the inlet. The maximum of the Gaussian distribution is (20µm).

C. Comparison of liquid velocity profiles

Droplet axial velocities are extracted from the simulation at a moment when the velocities are quasi-steady. This data is compared with experiments in Figure 4 and Figure 5. The obtained results are very encouraging. Indeed, the width of the velocity profile is correctly predicted. However, the simulation based on a constant droplet diameter overpredicts the velocity as expected. This is most probably due to the fact that secondary break-up and polydispersion are not accounted for. The main problem is that this simulation does not consider the large variance of droplet diameters that could be present in a spray and moreover it does not consider the evolution of the diameter along the spray axis.

This analysis is confirmed by the second simulation which provides a much more reasonable velocity profile. The results are improved since the radial distribution of diameter at the inlet is more realistic and in better accordance with literature [15].

Figure 5 presents the decrease of axial droplet velocity along spray axis. Simulations results are compared with an experimental formula given by Chaves [3] which fits well the experimental results. The results from the second simulation are in better agreement with the experimental formula because having a range of diameter in a monodisperse case leads to a diffusion effect of diameter. Then the mean droplet diameter along spray axis is decreasing by diffusion inherent to the Eulerian formalism. This proves the necessity of having an equation for the diameter

variance and correlations between droplets velocities and their diameters, i.e. the addition of polydispersion effects.

The picture of the spray given by Chaves (Figure 1) reveals pulsating structures induced by fluctuating velocity at the injector exit which is not considered. According to Chaves, these fluctuations can produce coherent structures and transport larger drops to the periphery of the spray resulting in peaks in the velocity profile which are not predicted by the simulation. These coherent structures are large enough to be resolved by the LES simulation. They are not reproduced because they are not triggered. The shifted boundary conditions omit the Kelvin-Helmholtz instabilities created by the shear flow at the nozzle exit. Thus the boundary conditions need to be adapted to meet this necessity. Future work will be focused on the development of unsteady boundary that allow to reproduce the effect of these instabilities.

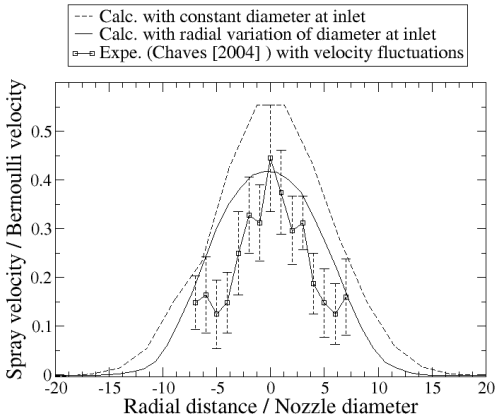

Figure 4 : Radial distribution of normalised axial droplet velocity at 100D from the injector nozzle

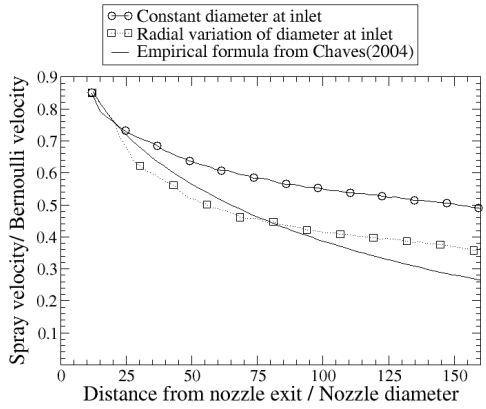

Figure 5 : Evolution of normalised axial droplet velocity on spray axis.

D. Contributions to the spray dynamics

Because of the multiple physical mechanisms involved in the spray behavior, one has to quantify their relative importance and contribution to the spray dynamics. For this purpose, the contribution terms to the spray momentum (rhs of Eq. (20)) are plotted on cut lines at 20D and 100D from the nozzle (Figure 1). This terms are projected in the axial direction (Figure 6 and Figure 7) and radial direction (Figure 8 and Figure 9). The contributions are normalized by the maximum of all the contributions for each projection. For the sake of simplicity we have selected the pressure like terms and viscous like terms. Bulk viscosity is omitted because it is negligible in our case. Drag force has the same order of magnitude as the maximum contribution and is not represented in this comparison. For all the graphs, the symbols are as follows :

- △ : term 1 in equation (20),
- ○ : term 2 in equation (20),
- □ : term 3 in equation (20),
- ◇ : term 4 in equation (20),
- ◁ : term 5 in equation (20).

E. Axial Contributions to the spray dynamics

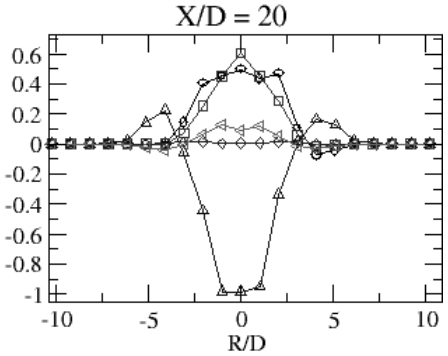

Figure 6 : Radial distribution of axial projection of contributions to spray momentum at 20D.

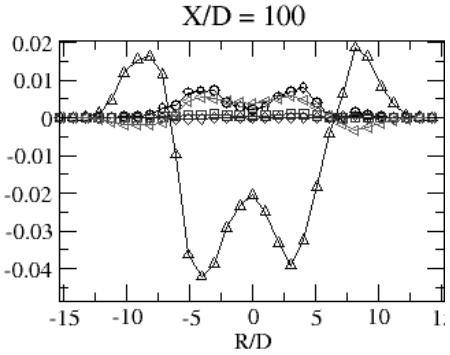

Figure 7 : Radial distribution of axial projection of contributions to spray momentum at 100D.

Figure 6 and Figure 7 show that the RUV viscous tensor adapted for collision is the prevailing term. Collisional terms have a significant importance especially at 20D (dense area). Liquid subgrid pressure is negligible**.**

F. Radial contributions to the spray dynamics

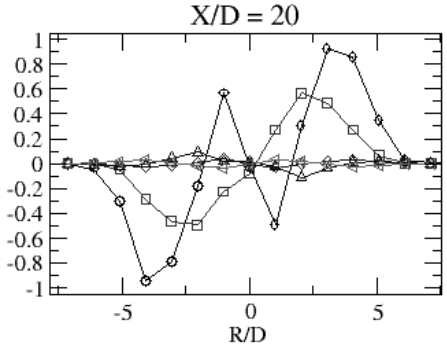

Figure 8 : Radial distribution of radial projection of contributions to spray momentum at 20D.

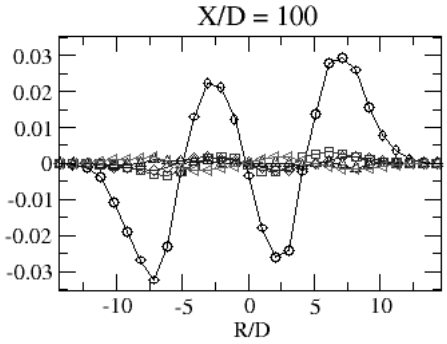

Figure 9 : Radial distribution of radial projection of contributions to spray momentum at 100D.

The radial projections presented on Figure 8 and Figure 9 show that the opening of the spray is mainly due to the RUV pressure and, especially in the dense area, to the collisional pressure. Liquid subgrid pressure is also negligible here**.** Without the RUV and collisional terms, the results for the spray velocity profiles plotted in Figure 4 would be less satisfactory, especially for the width of the spray.

Conclusions

The work presented in this paper represents a first step towards the application of LES on the simulation of two-phase flows in IC Diesel engines.

Indeed an Eulerian-Eulerian model has been adapted to the computation of dense sprays by taking into account the droplet-droplet interaction via bouncing collision and then validated on the experiment of Chaves [3].

Furthermore, the contribution of the different physical mechanisms considered in this model has also been analysed to determine which has the greatest influence on the spray dynamics. The effect of the RUM seems to be prevailing in the spray opening. Furthermore, the subgrid pressure for the liquid phase seems to be completely negligible in our case.

In order to avoid the numerical and physical difficulties involved in the simulation at the nozzle exit, a methodology consisting of initiating the calculation at ten nozzle diameters downstream from the nozzle exit is presented.

Nevertheless, the injector boundary conditions have to be improved by taking into account the unsteadiness of the flow and recreate the instabilities that could occur at the nozzle exit. This work is currently in progress.

References

[1] J. Bellan, Perspectives on Large Eddy Simulations for Sprays : Issues and Solutions, *Atomization and Sprays*, vol. 10, pp. 409-425, 2000.

[2] V. Moureau, G. Lartigue, Y. Sommerer, C. Angelberger, O. Colin, and T. Poinsot, Numerical methods for unsteady compressible multi-component reacting flows on fixed and moving grids, *J. Comp. Physics,* vol. 202, pp. 710-736, 2005.

[3] H. Chaves, C. Kirmse and F. Obermeier, Velocity measurements of dense Diesel fuel sprays in dense air, *Atomization and Sprays,* vol. 14, pp. 589-609, 2004

[4] P. Février, O. Simonin and K. Squires, Partionning of particle velocities in gas-solid flows into a continuous field and a spatially–uncorrelated random distribution : the theoretical and numerical study, *J. Fluid Mech.* vol. 533, 2005

[5] S. Chapman and T. Cowling. The mathematical theory of non-uniform gazes, *Cambridge mathematical library*, ed. Cambridge University Press*,* 1939 (digital reprint 1999).

[6] E. Riber M. Moreau, O. Simonin, and B. Cuenot, Development of Euler-Euler LES approach for gas-particle turbulent jet flow, *In FEDSM2006,* 2006.

[7] M. Moreau, B. Bédat, and O. Simonin, A priori testing of subgrid stress models for Euler-Euler two phase LES from Euler-Lagrange simulations of gas particle turbulent flow, *18th Ann. Conf. on Liquid Atomization and Sprays Systems,* 2005.

[8] O. Simonin, P. Février, and J. Laviéville, On the spatial distribution of heavy particle velocities in turbulent flow: from continuous field to particulate chaos, *J. Turbulence*, vol. 3, pp. 040, 2002.

[9] A. Kaufmann, O. Simonin, and T. Poinsot, Direct Numerical Simulation of particle-laden homogeneous isotropic turbulent flows using a two-fluid model formulation, *5th Int. Conf. on Multiphase Flow, ICMF'04*, 2004.

[10] H. Enwald, E. Peirano and A. Almstedt, Eulerian two-phase flow theory applied to fluidization, *Int. J. Multiphase Flow.* vol. 22, 1996.

[11] E. Peirano and B. Leckner, Fundamentals of turbulent gas-solid flows applied to circulating fluidized bed combustion, *Progress in Energy and Combustion Science*, vol. 24, pp 259-296, 1998.

[12] C. Lun and B. Savage, The effects of impact velocity dependent coefficient of restitution on stress developed by sheared granular materials, *Acta Mech.*, vol. 63, pp. 15-44, 1986.

[13] W. Sirignano, Volume averaging for the analysis of turbulent spray flows, *Int. J. Multiphase Flow.* vol. 31, pp. 675-705, 2005.

[14] G. Smallwood and O. Gulder, On the structure of transient diesel sprays, *Atomization and Sprays,* vol. *10*, pp. 355-386, 2000.

[15] H. Ueki, D. Ishida, M. Sakaguchi and M. Naganuma, Simultaneous Measurements of velocity and size of Diesel fuel near nozzle orifice by laser 2-focus velocimeter with micro-scale probe volume, *THIESEL 2004*, 2004.

[16] C. Sarre, S. Kong and R. Reitz, Modeling the Effects of Injector Nozzle Geometry on Diesel Sprays, *SAE PAPER 1999-01-0912*, 1999.

[17] A. Nishimura and D.N. Assanis. A Model for Primary Diesel Fuel Atomization Based on Cavitation Bubble Collapse Energy, *ICLASS2000.*

[18] K. Huh and A. Gosman, A phenomenological Model for Diesel Spray Atomization, *Int. Conference on Multiphase Flows'91*, 1991.